LETTER **Communicated by Bard Ermentrout**

Minimal Models of Adapted Neuronal Response to *In Vivo*–Like Input Currents

Giancarlo La Camera
lacamera@cns.unibe.ch
Alexander Rauch
rauch@pyl.unibe.ch
Hans-R. Lüscher
luescher@pyl.unibe.ch
Walter Senn
wsenn@cns.unibe.ch
Stefano Fusi
fusi@cns.unibe.ch
Institute of Physiology, University of Bern, CH-3012 Bern, Switzerland

Rate models are often used to study the behavior of large networks of spiking neurons. Here we propose a procedure to derive rate models that take into account the fluctuations of the input current and firing-rate adaptation, two ubiquitous features in the central nervous system that have been previously overlooked in constructing rate models. The procedure is general and applies to any model of firing unit. As examples, we apply it to the leaky integrate-and-fire (IF) neuron, the leaky IF neuron with reversal potentials, and to the quadratic IF neuron. Two mechanisms of adaptation are considered, one due to an afterhyperpolarization current and the other to an adapting threshold for spike emission. The parameters of these simple models can be tuned to match experimental data obtained from neocortical pyramidal neurons. Finally, we show how the stationary model can be used to predict the time-varying activity of a large population of adapting neurons.

1 Introduction

Rate models are often used to investigate the collective behavior of assemblies of cortical neurons. One early and seminal example was given by Knight (1972a), who described the difference between the instantaneous firing rate of a neuron and the instantaneous rate of a homogeneous population of neurons in response to a time-varying input. Ever since, more refined analyses have been developed, some making use of the so-called population density approach (see, e.g., Abbott & van Vreeswijk, 1993; Treves, 1993; Fusi & Mattia, 1999; Brunel & Hakim, 1999; Gerstner, 2000; Nykamp & Tranchina, 2000; Mattia & Del Giudice, 2002). The population activity

at time t is the fraction of neurons of the network emitting a spike at that time. In a homogeneous network of identical neurons and in stationary conditions, this population activity is the single neuron current-frequency (*f-I*) curve (the response function), which is accessible experimentally and has been the subject of many theoretical (Knight, 1972a; Amit & Tsodyks, 1991, 1992; Amit & Brunel, 1997; Ermentrout, 1998; Brunel, 2000; Mattia & Del Giudice, 2002) and in vitro studies (see, e.g., Knight, 1972b; Strafstrom, Schwindt, & Crill, 1984; McCormick, Connors, Lighthall, & Prince, 1985; Poliakov, Powers, Sawczuk, & Binder, 1996; Powers, Sawczuk, Musick, & Binder, 1999; Chance, Abbott, & Reyes, 2002; Rauch, La Camera, Lüscher, Senn, & Fusi, 2003). The *f-I* curve is central to much theoretical work on networks of spiking neurons and is a powerful tool in data analysis, where the population activity can be estimated by the peristimulus time histogram but requires many repetitions of the recordings under the same conditions. A suitable rate model would avoid this cumbersome and time-consuming procedure (see, e.g., Fuhrmann, Markram, & Tsodyks, 2002).

When the rate models are derived from detailed model neurons, the predictions on network behavior can be very accurate. Recently Shriki, Hansel, and Sompolinsky (2003) fitted a rate model to the *f-I* curve of a conductance-based neuron with Hodgkin-Huxley sodium and potassium conductances and an A-current. The A-current was included to linearize the *f-I* curve as observed in experiment. With their model, Shriki et al. (2003) can predict, in several case studies, the behavior of the network of neurons from which the rate model was derived.

A similar approach was taken by Rauch et al. (2003), who fitted the response functions of white noise–driven IF neurons to the *f-I* curves of rat pyramidal neurons recorded in vitro. They found that firing-rate adaptation had to be included in the model in order to fit the data. As opposed to the approach of Shriki et al. (2003), the contribution of the input fluctuations to the output rate was taken explicitly into account. Here we present a general scheme to derive adapting rate models in the presence of noise, of which the model used by Rauch et al. (2003) is a special case.

The general scheme that we introduce may be considered a generalization of a model due to Ermentrout (1998). This author introduced a general rate model in which firing-rate adaptation is due to a feedback current; that is, the adapted rate f is given as the self-consistent solution of the equation $f = \Phi(I - \alpha f)$, where I is the applied current, Φ is the *f-I* curve in stationary conditions, and α is a parameter that quantifies the strength of adaptation. In this model, the effect of noise is not considered. For most purposes, the input to a cortical neuron can be decomposed in an average component, m, and a fluctuating gaussian component whose amplitude is quantified by its standard deviation, s, and the response of the neuron can be expressed as a function of these two parameters (see, e.g., Ricciardi, 1977; Amit & Tsodyks, 1992; Amit & Brunel, 1997; Destexhe, Rudolph, Fellous, & Sejnowski, 2001).

We show that under such conditions, Ermentrout's model can be easily generalized, and the adapted response can be obtained as the fixed point of $f = \Phi(m - \alpha f, s)$. For this result to hold, it is necessary that adaptation is slow compared to the timescale of the neural dynamics. In such a case, the feedback current αf is a slowly fluctuating variable and does not affect the value of s. Note that a slow adaptation is a minimal request in the absence of noise (Ermentrout, 1998).

The proposed model is very general, but it can be used to full advantage only if the response function Φ is known analytically. This is the case of simple model neurons, for which the rate function can be calculated, or more complex neurons whose *f-I* curve can be fitted by a suitable model function (e.g., Larkum, Senn, & Lüscher, in press). In section 2, the adapting rate model is introduced and tested on several versions of IF neurons, whose rate functions are known and easily computable. The resulting rate models are checked against the simulations of the full models from which they are derived, including the leaky IF (LIF) neuron with conductance-based synaptic inputs. Only slight variations are needed if a different mechanism of adaptation is considered, as, for example, an adapting threshold for spike emission, which is dealt with in section 2.2. Evidence is also provided that the LIF neuron with an adapting threshold is able to fit the response functions of rat pyramidal neurons (see section 2.3), a result that parallels those of Rauch et al. (2003) obtained with an afterhyperpolarization current. Finally, in section 3, we show how the stationary response function can be used to predict the time-varying activity of a large population of adapting neurons.

2 Adapting Rate Models in the Presence of Noise

Firing-rate adaptation is a complex phenomenon characterized by several timescales and affected by different ion currents. At least three phases of adaptation have been documented in many in vitro preparations, referred to as initial or one-interspike (ISI) interval adaptation, which affects the first or at most the first two ISIs (Schwindt, O'Brien, & Crill, 1997), early adaptation, involving the first few seconds, and late adaptation, shown in response to a prolonged stimulation (see Table 1 of Sawczuk, Powers, & Binder, 1997, for references and a list of possible mechanisms).

Initial adaptation depends largely on Ca^{2+}-dependent K^+ current (Sah, 1996; Powers et al., 1999), although other mechanisms may also play a role (Sawczuk et al., 1997). The early and late phases of adaptation are not well understood, and several mechanisms have been put forward: in neocortical neurons, it seems that Na^+-dependent K^+ currents (Schwindt, Spain, & Crill, 1989; Sanchez-Vives, Nowak, & McCormick, 2000), and slow inactivation of Na^+ channels (Fleidervish, Friedman, & Gutnik, 1996) may play a major role; in motoneurons, evidence is accumulating for an interplay between slow inactivation of Na^+ channels, which tend to decrease the firing rate,

and the slow activation or facilitation of a calcium current, which tends to increase the discharge rate (Sawczuk et al., 1997; Powers et al., 1999).

Despite the many mechanisms involved, we derive in the following a simple model for the adapted rate at steady state, which describes synthetically the overall phenomenology. The cellular mechanism is inspired by those mentioned above: upon emission of a spike, a quantity A_N of a given ion species N (one can think of Ca^{2+} or Na^{+}) enters the cell and modifies the intracellular ion concentration $[N]_i$, which then exponentially decays to its resting value in a characteristic time τ_N. Its dynamics are described by

$$\frac{d[N]_i}{dt} = -\frac{[N]_i}{\tau_N} + A_N \sum_k \delta(t - t_k), \tag{2.1}$$

where the sum is taken over all the spikes emitted by the neuron up to time t. As a consequence, an outward, N-dependent current $I_{ahp} = -g_N[N]_i$, proportional to $[N]_i$ through the average peak conductance g_N, results and causes a decrease in the discharge rate. Following the literature, we give this current the name of afterhyperpolarization (AHP) (e.g., Sah, 1996).

Experimentally, the time constant τ_N of the dynamics underlying AHP summation (see equation 2.1) is found to be of the order of tens of milliseconds (fast AHP), hundreds of milliseconds to a few seconds (medium-duration AHP), to seconds (slow AHP) (see, e.g., Powers et al., 1999). Values often used in modeling studies are of the order of 100 ms (Wang, 1998; Ermentrout, 1998; Liu & Wang, 2001). In all cases, N-dynamics is typically slower than the average ISI. This fact can be exploited to obtain the stationary, adapted output frequency by noticing that from equation 2.1, the steady state (ss) intracellular concentration would be proportional to the neuron's output frequency in a time window of a few τ_N:

$$[N]_{i,ss} = \tau_N A_N \sum_{t_k<T} \delta(t - t_k) \approx \tau_N A_N f,$$

where $T \gg \tau_N$. This causes a feedback current $I_{ahp,ss}$ proportional to $[N]_{i,ss}$, $I_{ahp} = -g_N[N]_{i,ss}$, which is in general a fluctuating variable, as the output spike train is. We assume the neuron to be driven by a fluctuating current that can be described as an average component m plus a fluctuating component with zero mean and variance s^2. If the current is gauss distributed, as we always assume in this article, m and s^2 are sufficient to characterize the current. Since $[N]_i$ dynamics are slow, $I_{ahp,ss}$ is only weakly fluctuating compared to the input current, so that only m is significantly affected. The total current felt by the neuron, spiking at frequency f, is then $m - \alpha f$, with $\alpha = g_N \tau_N A_N$, plus the fluctuating component, which is unaffected by adaptation. This would cause the neuron to fire at a reduced frequency f_1, which in turn causes the mean current to be affected as $m - \alpha f_1$, and so on. At equilibrium, the adapted frequency can be numerically obtained by solving

the self-consistent equation

$$f = \Phi(m - \alpha f, s), \tag{2.2}$$

which requires only the knowledge of the response function Φ (the actual dynamics leading to equation 2.2 is dealt with in more detail in section 3). It is easy to prove that the adapted firing rate, f_α, is always a stable fixed point of equation 2.2: the condition for stability reads $\Lambda \equiv \partial_f \Phi(m - \alpha f, s)|_{f_\alpha} < 1$; for equation 2.2, one has $\Lambda = -\alpha \partial_m \Phi(m - \alpha f, s)|_{f_\alpha} < 0$, as $\alpha > 0$ and Φ is an increasing function of m.

2.1 Examples. We checked the rate model, equation 2.2, against full simulations for several versions of IF neurons. In each case, the rate function in the presence of noise, Φ, is known.

2.1.1 Leaky Integrate-and-Fire Neuron. The leaky integrate-and-fire (LIF) neuron is the best-known and most widely used of all IF neurons (see section A.1 for details of the model). Its response function in the presence of noise has been known for a long time; it reads

$$\Phi_{LIF}(m, s) = \left[\tau_r + \tau \int_{\frac{CV_r - m\tau}{\sigma\sqrt{\tau}}}^{\frac{C\theta - m\tau}{\sigma\sqrt{\tau}}} \sqrt{\pi} e^{x^2} (1 + \mathrm{erf}(x)) dx \right]^{-1} \tag{2.3}$$

(Siegert, 1951; Ricciardi, 1977; Amit & Tsodyks, 1991). V_r and τ_r are the reset potential and the absolute refractory period after spike emission, which is said to occur when the membrane potential hits a fixed threshold θ; τ is the membrane time constant; C is the membrane capacitance; and erf(x) $= (2/\sqrt{\pi}) \int_0^x dt e^{-t^2}$ is the error function. m and $\sigma = \sqrt{2\tau'} s$ are the average current and the amplitude of the fluctuations, with s in units of current and τ' a time constant to preserve units (set equal to 1 ms throughout).

The equivalence between the rate model and the full simulation for different values of the noise is shown in Figure 1A. We report also the lower bound for the time constant (around $\tau_N \sim 80$ ms) for which the result holds (see Figure 1B). For irregular spike trains the agreement is remarkable also at very low frequencies, where the condition that the average ISI be smaller than τ_N is violated. This may be explained by the fact that although <ISI> $> \tau_N$, the ISI distribution is skewed towards smaller values, and $I_{alp} \sim -\alpha f$ is still a good approximation.

2.1.2 Quadratic Integrate-and-Fire Neuron. The quadratic integrate-and-fire (QIF) neuron—see section A.2—is related to a canonical model of type I membrane (see, e.g., Ermentrout & Kopell, 1986; Ermentrout, 1996). As such, it is expected to reproduce the firing behavior of any type I neuron close to

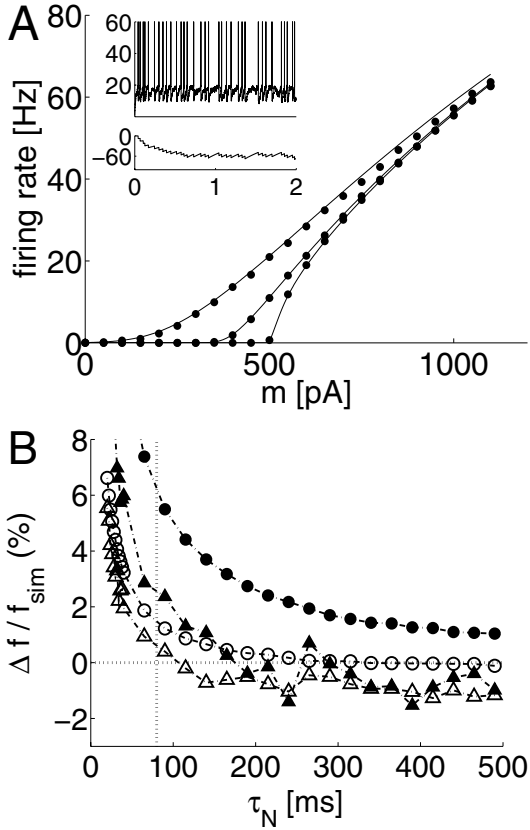

Figure 1: Adapting rate model from the LIF model neuron, theory versus simulations. (A) rate functions of adapted LIF neuron. Plots show firing rate as a function of the mean current m at constant noise $s = 0, 200$ and 600 pA (from right-most to left-most curve). Lines: Self-consistent solutions of equation $f = \Phi_{LIF}(m - \alpha f, s)$ (f_{th}), with Φ_{LIF} given by equation 2.3. Dots: Simulations of the full model, equations 2.1 and A.1 (f_{sim}). Adaptation parameters: $\tau_N = 500$ ms, $g_N A_N = 8$ pA (so that $\alpha = 4$ pA·s). Neuron parameters: $\tau_r = 5$ ms, $C = 500$ pF, $\theta = 20$ mV, $V_r = 10$ mV, $V_{rest} = 0$, $\tau = 20$ ms. Inset: Sample of membrane voltage (mV, top trace) and feedback current I_{alp} (pA, bottom trace) as a function of time (in seconds) for the input point $(m, s) = (550, 200)$ pA. Note how equilibrium is reached after $\approx 1s = 2\tau_N$. (B) Dependence of $(f_{sim} - f_{th})/f_{sim}$ on τ_N. As τ_N is varied, A_N is rescaled so that the total amount of adaptation ($\alpha = 4$ pA·s) is kept constant. Parameters of the current: $m = 600$ pA (full symbols) and $m = 800$ pA (empty symbols); $s = 0$ (circles) and $s = 200$ pA (triangles). All other parameters as in A. Mean spike frequencies assessed across 50 s, after discarding a transient of $10\tau_N$. Integration time step $dt = 0.1$ ms. For $s > 0$, finite noise effects have to be expected, but the error is always below 3%. For $\tau_N < 80$ ms, the error is positive, meaning that $f_{sim} > f_{th}$: the neuron adapts only slightly because N decays too quickly (vertical dotted line: 80 ms).

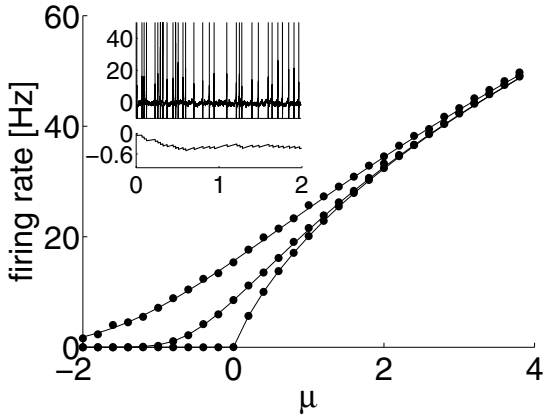

Figure 2: Adapting rate model from the QIF neuron, theory versus simulations. *f-I* curves plotted as in Figure 1A. Lines: Self-consistent solutions of equation $f = \Phi_{QIF}(\mu - \alpha f, \sigma)$, with Φ_{QIF} given by equation 2.4. Dots: Simulations of the full model, equations 2.1 and A.2 (f_{sim}). Parameters: $\tau_N = 500$ ms, $g_N A_N = 0.06$ ($\alpha = 0.03$ s), $\tau = 20$ ms, $\tau_r = 0$; $\sigma = 0, 0.8, 1.6$ (from right to left). Inset: Same as in Figure 1A, for the point $(\mu, \sigma) = (-0.2, 1.6)$. Mean spike frequencies f_{sim} assessed across 50 s, after discarding a transient of $10\tau_N$.

bifurcation, where the firing rates are low. Its firing rate in the presence of white noise reads

$$\Phi_{QIF} = \left[\tau_r + \sqrt{\pi}\,\tau \int_{-\infty}^{+\infty} dx \exp\left(-\mu x^2 - \frac{\sigma^2 x^6}{48} \right) \right]^{-1}, \tag{2.4}$$

(see Brunel & Latham, 2003). μ and σ quantify the drift and the fluctuations of a (dimensionless) gaussian input current. The adapted response in stationary conditions is given by $f = \Phi_{QIF}(\mu - \alpha f, \sigma)$. The match between the predictions of the adapting rate model and simulations of the QIF neuron is presented in Figure 2.

2.1.3 Conductance-Based IF Neuron. The scenario outlined so far considered only current-based model neurons—models in which the input current does not depend on the state of the membrane voltage. A more realistic description takes into account the dependence of the current on the reversal potentials, $V_{E,I}$, for the excitatory and inhibitory inputs, respectively. The adapting rate model for this class of neurons can be derived in the same way as done for the current-based models. For the LIF neuron with reversal potentials defined in section A.3, and referred to as the conductance-based (CB) neuron in the following, one finds that the adapted response is the

fixed point of the self-consistent equation,

$$f = \Phi_{CB}(m_0 - \alpha f, s_0), \tag{2.5}$$

where

$$\Phi_{CB} = \left[\tau_r + \tau^* \int_{\frac{CV_r - m_0\tau^*}{s_0\sqrt{\tau^*}}}^{\frac{C\theta - m_0\tau^*}{s_0\sqrt{\tau^*}}} \sqrt{\pi} e^{x^2} (1 + \mathrm{erf}(x)) dx \right]^{-1}. \tag{2.6}$$

Φ_{CB} is the rate function of the CB neuron (Burkitt, Meffin, & Grayden, 2003). Note that the only difference with the response function of the current-based LIF neuron, equation 2.3, is in the dependence of the quantities m_0, s_0, τ^*, given, respectively, by equations A.10, A.11, and A.6, upon the input parameters $\bar{g}_{E,I}$, $\nu_{E,I}$. Here $\bar{g}_{E,I}$ are the excitatory and inhibitatory peak conductances and $\nu_{E,I}$ the mean frequencies of the input spike trains, modeled as Poisson processes. Equations A.10 and A.11 have to be compared with

$$m = \bar{g}_E \nu_E - \bar{g}_I \nu_I, \qquad s^2 = \bar{g}_E^2 \nu_E + \bar{g}_I^2 \nu_I,$$

valid for the current-based neuron. Note that one way to obtain the plots of Figure 1A is to increase ν_E while scaling $\bar{g}_E$ as $A/\sqrt{\nu_E}$, with A held constant and for constant inhibition (i.e., for constant $\bar{g}_I$, ν_I). This in fact corresponds to increasing m as $A\sqrt{\nu_E} - \bar{g}_I \nu_I$ at constant noise $s^2 = A^2 + \bar{g}_I^2 \nu_I$. To make a comparison with the current-based neuron, we plotted Φ_{CB} as a function of $\mu_E = \bar{g}_E \nu_E$ according to such a procedure in Figure 3, which presents the match between the predictions of the rate model and simulations of the adapting CB neuron.

2.1.4 Other Model Neurons. A similar agreement is obtained for other IF model neurons (results not shown). Particularly worth mentioning is the constant leakage IF neuron with a floor (CLIFF) (Fusi & Mattia, 1999; Rauch et al., 2003), whose response function is very simple and does not require any integration:

$$\Phi(m, s) = \left[\tau_r + \frac{\sigma^2}{2(m - \lambda)^2} \left(e^{-\frac{2C\theta(m-\lambda)}{\sigma^2}} - e^{-\frac{2CV_r(m-\lambda)}{\sigma^2}} \right) + \frac{C(\theta - V_r)}{m - \lambda} \right]^{-1}.$$

The input parameters m, σ are defined as for the LIF neuron. The CLIFF neuron is an LIF neuron with constant leakage (i.e., with the term $-(V - V_{rest})/\tau$ in equation A.1 replaced by the constant $-\lambda/C$), and a reflecting barrier for the the membrane potential (Fusi & Mattia, 1999).

However, the scheme proposed here to derive the adapting rate models does not apply to IF neurons only. For example, the response function of a Hodgkin-Huxley neuron with an A-current can be fitted by the simple model $\Phi_1 = a[m - m_{th}]_+ - b[m - m_{th}]_+^2$ (Shriki et al., 2003), where a, b

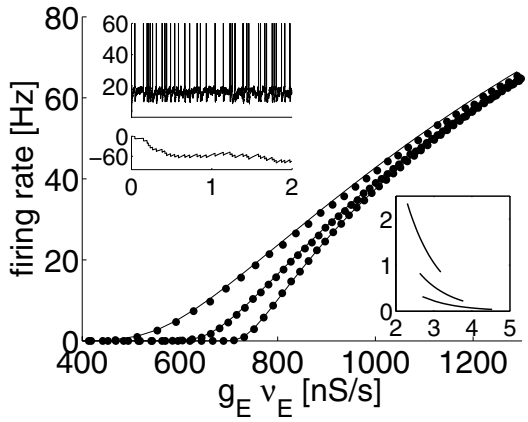

Figure 3: Adapting rate model from the conductance-based LIF neuron, theory versus simulations. Lines: Self-consistent response of equation 2.5 plotted as $\bar{g}_E \nu_E \rightarrow f$ at constant inhibition, with $\nu_I = 500$ Hz, $\bar{g}_I = 1$ nS throughout. Dots: Simulations of the full models (f_{sim}). Each curve is obtained moving along ν_E and scaling $\bar{g}_E$ so that $\sigma_E^2 \equiv \bar{g}_E^2 \nu_E$ constant, to allow comparison with the current-based neurons in Figure 1A. $\bar{g}_E$ [nS] as a function of ν_E [Hz] shown in the right inset as $\bar{g}_E$ vs $\log_{10}(\nu_E)$. The resulting σ_E values were 7.0, 16.9, 33.1 nS/$\sqrt{\text{s}}$ (from right to left). Adaptation and neuron parameters as in Figure 1A, plus $V_E = 70$ mV, $V_I = -10$ mV. Left inset as in Figure 1 with $\mu_E = 783$ nS/s, $\sigma_E = 33.1$ nS/$\sqrt{\text{s}}$. Mean spike frequencies f_{sim} assessed across 50 s, after discarding a transient of $10\tau_N$.

are two positive constants (such that $\Phi_1 \geq 0$ always), the rheobase m_{th} is an increasing function of the leak conductance g_L (Holt & Koch, 1997), and $[x]_+ = x$ if $x > 0$, and zero otherwise. The adapting rate model that corresponds to Φ_1, that is, $f = \Phi_1(m - \alpha f; a, b, g_L)$, could be interpreted as the rate model for the Hodgkin-Huxley neuron underlying it.

Another example is given by the function $\Phi_2 \propto \sqrt{[m - m_{th}]_+}$, which describes the firing behavior of a type I membrane close to bifurcation and has been fitted (Ermentrout, 1998) to the in vitro response of cells from cat neocortex in the absence of noise (Stafstrom et al., 1984), and to the Traub model (Traub & Miles, 1991). It is easily seen that Φ_2 is the rate function of the QIF neuron when $\sigma = 0$. Like Φ_1, this model does not take fluctuations explicitly into account.

2.1.5 IF Neurons with Synaptic Dynamics. The adapting rate model also works in the presence of synaptic dynamics, provided that the appropriate response function is used. For example, for the LIF neuron with fast synaptic dynamics, this is equation 2.3 with $\{\theta, V_r\}$ replaced by $\{\theta, V_r\} + 1.03 s_v \sqrt{\tau_s/\tau}$,

where s_v is the standard deviation of the input in units of voltage and $\tau_s \ll \tau$ is the synaptic time constant (Brunel & Sergi, 1998; Fourcaud & Brunel, 2002). This model will be used in section 3, which deals with time-dependent inputs. For slow synaptic dynamics, the response of the LIF neuron has been given by Moreno-Bote and Parga (2004b), while the response of the QIF neuron in both regimes has been given by Brunel and Latham (2003).

2.2 The Adapting Threshold Model. The above construction can be applied to other models in which the adaptation mechanism is of a different type. Among those is a model in which the threshold for spike emission adapts (see, e.g., Holden, 1976; Wilbur & Rinzel, 1983; Liu & Wang, 2001).

In the adapting threshold model, the emission of an action potential causes the threshold θ for spike emission to step increase by an amount B_θ and then exponentially decay to its resting value θ_0 with a time constant τ_θ:

$$\frac{d\theta}{dt} = -\frac{\theta - \theta_0}{\tau_\theta} + B_\theta \sum_k \delta(t - t_k). \tag{2.7}$$

There is indeed evidence that the spike threshold rises after the onset of a current step (Schwindt & Crill, 1982; Powers et al., 1999). Note that the feedback now affects the threshold, not the current. This case can be handled in a similar way as done for AHP adaptation: after a transient of the order of τ_θ, the neuron will have an average threshold proportional to its own output frequency,

$$\theta \approx \theta_0 + B_\theta \tau_\theta f \equiv \theta_0 + \beta f,$$

with $\beta = B_\theta \tau_\theta$, and the adapted response f is given by the self-consistent solution of

$$f = \Phi(\theta_0 + \beta f; m, s). \tag{2.8}$$

Also, this reduction is expected to work for slow enough threshold dynamics, $\tau_\theta \sim 100$ ms, but apart from that, at any output frequency. This is confirmed by Figure 4, in which the prediction of the rate model is checked against the simulations of the full model for the LIF neuron (that is, equation 2.7 and equation A.1 with $I_{alpha} = 0$). A similar agreement is obtained for the conductance-based LIF neuron (not shown). The qualitative differences between the two adapting models for the LIF neuron are illustrated in the next section, where we report the results of fitting the response functions to those of cortical pyramidal neurons.

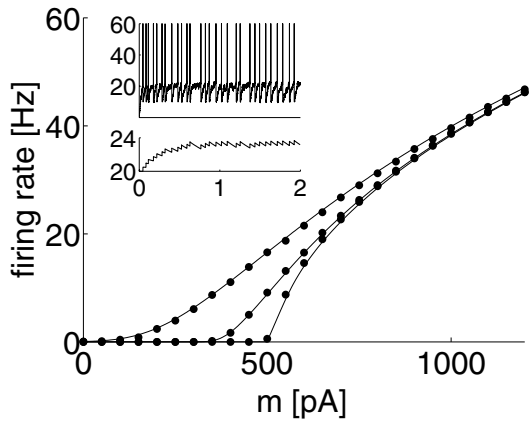

Figure 4: LIF neuron with an adapting threshold, theory versus simulations. *f-I* curves plotted as in Figure 1A. Lines: Self-consistent solutions of equation $f = \Phi(\theta_0 + \beta f, s)$, with Φ given by equation 2.3. Dots: Simulations of the full model, equations 2.7 and A.1, (f_{sim}). Adaptation parameters: $\tau_\theta = 500$ ms, $B_\theta = 0.5$ mV·s (so that $\beta = 0.25$ mV·s). Neuron parameters and s values as in Figure 1A. Inset: Sample of membrane potential and $\theta(t)$ for the point $(m, s) = (550, 200)$ pA (time in seconds). Note that for this point, the output frequency is $f \approx 14$ Hz, so that after the transient $\langle\theta\rangle = \theta_0 + \beta f \approx 23.5$ mV, as shown in the inset. Mean spike frequencies f_{sim} assessed across 50 s, after discarding a transient of $10\tau_\theta$.

2.3 Quantitative Comparison with Experimental Data. We have shown previously that the LIF neuron with AHP adaptation can be fitted to the experimental response functions of rat pyramidal neurons under noisy current injection (Rauch et al., 2003). We extended the analysis to the LIF neuron with an adapting threshold to find basically the same result. The results for the 26 rat pyramidal neurons considered for the analysis are summarized in Table 1 (see appendix B for details). Two examples are shown in Figure 5.

The two adapting models can be made equivalent in the region of low frequencies, being both threshold-linear with slopes $1/\alpha$ (AHP) and $\tau/C\beta$ (adapting threshold; see appendix C for details). This is confirmed by Table 1, which shows that C and τ are the same for the two models and $C\beta/\tau = 4.46$ pA·s, consistent with $\alpha = 4.3 \pm 2.2$.

The two models differ in the value of the refractory period, which is much shorter for the adapting threshold model. In fact, imposing $\tau_r = 0$ only marginally affects the quality of the fits. This is because the LIF neuron with an adapting threshold has a square root behavior in m at intermediate and large frequencies (see equation C.1). To the contrary, a refractory period

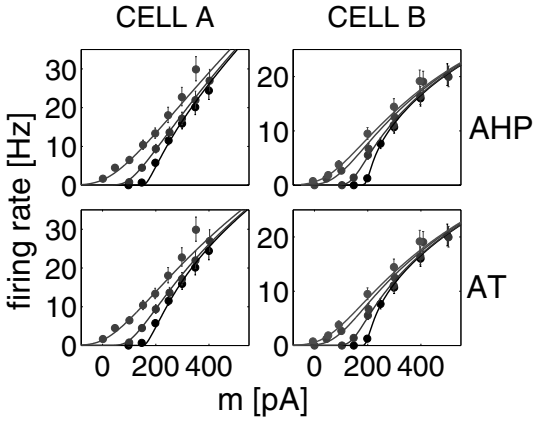

Figure 5: Best fits of different models to the rate functions of two rat pyramidal cells (see appendix B). Models: LIF neuron with AHP adaptation (AHP) and with an adapting threshold (AT). Theoretical curves (full lines) and experimental points (dots) plotted as in Figure 1A. Best-fit parameters are: Cell A: AHP: $\tau_r = 6.6$ ms, $\tau = 27.1$ ms, $C = 260$ pF, $V_r = 1.7$ mV, $\alpha = 5.1$ pA·s, $P = 0.32$; AT: $\tau_r = 2.2$ ms, $\tau = 28.8$ ms, $C = 270$ pF, $V_r = 14$ mV, $\beta = 0.58$ mV·s, $P = 0.38$. Cell B: AHP: $\tau_r = 19.8$ ms, $\tau = 41.1$ ms, $C = 440$ pF, $V_r = -2$ mV, $\alpha = 2.8$ pA·s, $P = 0.85$; AT: $\tau_r = 6.8$ ms, $\tau = 40.1$ ms, $C = 430$ pF, $V_r = -12.8$ mV, $\beta = 0.30$ mV·s, $P = 0.80$. In all the fits, the threshold (θ_0 in AT) was kept fixed to 20 mV. P equals the probability that χ^2 is larger than the observed minimum $\chi^2_{\min}$. The fit was accepted whenever $P > 0.01$. Amplitude of the fluctuating current: cell A: $s = 0$, 200 and 400 pA; cell B: $s = 50$, 200, 400 and 500 pA.

is required to bend the response of the model with AHP, otherwise linear in that region.

3 Adapting Response to Time-Dependent Inputs

The stationary response function can be used also to predict the time-varying activity of a population of adapting neurons, as shown in this section. Consider an input spike train of time-varying frequency $\nu_x(t)$, targeting each cell of the population through x-receptor mediated channels. Each spike contributes a postsynaptic current of the form $\bar{g}_x e^{-t/\tau_x}$, where $\bar{g}_x$ is the peak conductance of the channels. In the diffusion approximation, such an input I_x is an Ornstein-Uhlenbeck (OU) process with average $\bar{m}_x = \bar{g}_x \nu_x(t)\tau_x$, variance $\bar{s}_x^2(t) = (1/2)\bar{g}_x^2 \nu_x(t)\tau_x$, and correlation length τ_x:

$$dI_x = -\frac{I_x - \bar{m}_x}{\tau_x} dt + \bar{s}_x \xi_t \sqrt{\frac{2dt}{\tau_x}}, \tag{3.1}$$

where ξ_t is the unitary gaussian process defined in section A.1.

Table 1: Summary of the Results of the Fit of the LIF Neuron to the Experimental Rate Functions of 26 Rat Neocortical Pyramidal Cells.

	AHP	**AT**
N	14	13
α [pA · s], β [mV · s]	4.3 ± 2.2	0.29 ± 0.13
τ_r [ms]	9.0 ± 6.5	3.0 ± 4.0
τ [ms]	33.2 ± 9.4	32.5 ± 9.2
C [nF]	0.50 ± 0.18	0.50 ± 0.18
V_r [mV]	0.1 ± 11.2	1.1 ± 13.7
P	0.40 ± 0.30	0.33 ± 0.29

Notes: N is the number of fitted cells that required an adaptation parameter (α, or β) > 0. Two cells could be fitted without adaptation and were not included in the analysis. The parameters (left-most column) are defined in section 2.1 and their best-fit values are reported as average $\pm$ SD. The threshold for spike emission was held fixed to 20 mV. P is the probability $P[\chi^2 > \chi^2_{\min}]$ across fitted cells requiring adaptation. A fit was accepted whenever $P > 0.01$. The threshold for spike emission was held fixed to 20 mV. *AT*: adapting threshold model.

The population activity of noninteracting neurons is well predicted by $f(t) = \Phi(m_x, s_x^2)$, where Φ is the stationary response function, and m_x, s_x^2 are the time-varying average and variance of I_x (see, e.g., Renart, Brunel, & Wang, 2003). These evolve according to the first-order dynamics ($\dot{y} \equiv dy/dt$),

$$\tau_x \dot{m}_x = -(m_x - \bar{m}_x), \tag{3.2}$$

and analogously for s_x^2, with τ_x replaced by $\tau_x/2$ (e.g., Gardiner, 1985). We now include adaptation in the following way:

$$\begin{aligned} f &= \Phi(m_x - I_{ahp}, s_x^2) \\ \tau_N \dot{I}_{ahp} &= -I_{ahp} + \alpha f, \end{aligned} \tag{3.3}$$

where I_{ahp} is the AHP current, which follows the instantaneous output rate with time constant τ_N. Note that for a stationary stimulus, that is, ν_x constant, after a transient of the order of $\max\{\tau_x, \tau_N\}$, one recovers the stationary model, equation 2.2, with $m = \bar{m}_x$, $s = \bar{s}_x$.

In the case of several independent components, they follow their own synaptic dynamics and sum up in the argument of the response function to give the time-varying firing rate:

$$f = \Phi\left(\sum_x m_x - I_{ahp}, \sum_x s_x^2\right).$$

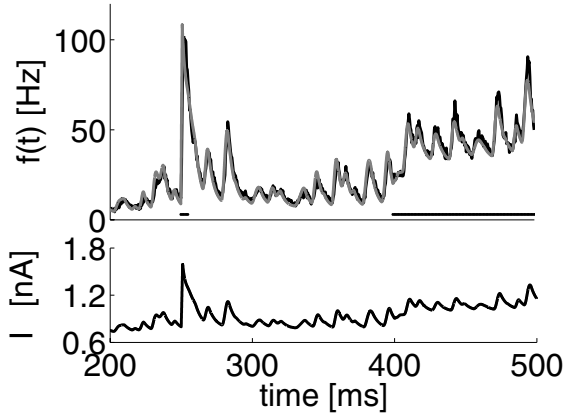

Figure 6: Time-varying activity of a population of independent, adapting LIF neurons in response to a noisy, broadband stimulus. (Top) prediction of the adapting rate model, equation 3.4 (gray), compared to the simulations of 20,000 neurons (black), as described in section 3. Shown is the activity after a transient of 200 ms. The short horizontal bar indicates a pulselike increase of 1 ms duration in ν_0, of strength $12\nu_0$. The long horizontal bar indicates a 50% steplike increase in ν_0, during which the inhibitory rate step increases by $0.7\nu_0$. (Bottom) Average time course of the stimulus. Neuron parameters as in Figure 1a, apart from $\tau_r = 2$ ms. Other parameters (refer to the text): $\nu_0 = 350$ Hz, $\nu_{inh} = 1.2\nu_0$, $G_{ampa,gaba} = 200$ pA, $G_{nmda} = 10$ pA, $\tau_{ampa,gaba} = 5$ ms, $\tau_{nmda} = 100$ ms. Bin size of the PSTH: 0.5 ms. Integration time step: 0.01 ms.

In Figure 6 we show an example with two fast ($\tau_x = 5$ ms) components, one excitatory (AMPA-like), the other inhibitory (GABA$_A$-like), plus a third component mimicking slow (NMDA-like) current (with $\tau_{nmda} = 100$ ms). The latter component is only slowly fluctuating, so that its variance can be neglected (Brunel & Wang, 2001), as in the case of the adaptation current. The output rate was calculated as

$$f(t) = \Phi(m_{ampa} + m_{nmda} - m_{gaba} - I_{ahp}, s^2_{ampa} + s^2_{gaba}), \tag{3.4}$$

where Φ is equation 2.3 corrected for fast synaptic dynamics (Fourcaud & Brunel, 2002), see section 2.1.5. The excitatory stimulus was of the form $\nu_0(1+\Delta(t))$, with $\nu_0 = 350$ Hz and $\Delta(t)$ a rectified superposition of 10 sinusoidal components with random frequencies $\omega_i/2\pi$, phases ϕ_i, and amplitudes A_i drawn from uniform distributions (the latter between 0 and 0.5):

$$\Delta(t) = \left[\sum_i A_i \sin(\omega_i t + \phi_i)\right]_+ .$$

The maximum value used for $\omega/2\pi$ was 150 Hz. ν_I was held constant to $1.2\nu_0$. This gives $\bar{m}_{ampda,nmda} = \bar{g}_{ampa,nmda}\nu_0(1 + \Delta(t))\tau_{ampa,nmda}$, $\bar{m}_{gaba} = 1.2\bar{g}_{gaba}\nu_0\tau_{gaba}$, with m_x given by equation 3.2, and analogously for $s^2_{ampa,gaba}$. The input currents used in the simulations were $[I_x]_+$, where I_x evolved according to the OU process, equation 3.1. Each neuron received an independent realization of the stochastic currents. The time-varying population activity was assessed through the peristimulus time histogram (PSTH) with a bin size of 0.5 ms. The model makes a good prediction of the population activity, even during fast transients, as in response to the impulse of 1 ms duration at $t = 250$ ms and a step increase in ν_0, ν_{inh} occurred at $t = 400$ ms (horizontal bars in Figure 6). The small discrepancies are due to finite size effects (Brunel & Hakim, 1999; Mattia & Del Giudice, 2002), and to the approximation used for the stationary response function.

Similar results were obtained with the adapting threshold model (i.e., with $I_{ahp} = 0$ and equation 3.3 replaced by $\tau_\theta\dot{\theta} = -(\theta - \theta_0) + \beta f$), and for the CB neuron (not shown). It has to be noticed that the condition $\tau_{ampa,gaba} \ll \tau^*$, where τ^* is the effective time constant of the CB neuron (see equation A.6), is usually more difficult to fulfill, as τ^* can reach values as small as a few ms, depending on the input (see, e.g., Destexhe et al., 2001). However, when $\tau^* < \tau_{ampa,gaba}$, a good approximation to the response function has been given by Moreno-Bote and Parga (2004a).

4 Discussion

We have proposed a general scheme to derive adapting rate models in the presence of fluctuating input currents. The adapting rate model is a reduced two-dimensional model that is a minimal model to fit the response of cortical neurons to in vivo–like current with stationary distribution. The rate models are easily computable; reproduce well the simulations of the full models from which they are derived; are of wide applicability (e.g., apply to model neurons with conductance-based synaptic inputs); allow for different mechanisms of adaptation to be used; and can be used to predict the activity of a large population of adapting spiking neurons in response to time-varying inputs. We considered an AHP current and an adapting threshold for spike emission, two mechanisms for which there is experimental evidence and which are often used in modeling studies. The only requirement is that adaptation be slow compared to the scale of the neural dynamics.

Since the adapting rate models (with either model of adaptation) considered in this study are able to fit the rate functions of neocortical neurons, they offer a synthetic way to describe cortical firing, and the diversity of possible models can be used for a quantitative (and possibly functional) classification of cortical neurons based on their observed response to in vivo–like currents.

Since the stationary model predicts the time-varying activity of a large population of independent neurons, the response function measured by Rauch et al. (2003) can be used to make quantitative analyses of the population dynamics, and not only of the stationary states (Amit & Brunel, 1997; Mattia & Del Giudice, 2002). This is particularly the case for networks of neurons in the fluctuation-dominated regime (e.g., Shadlen & Newsome, 1998; Fusi & Mattia, 1999), when spikes are emitted because of large fluctuations of the membrane potentials around an average value that is below the threshold. Such a regime could be the consequence of a high-conductance state (Destexhe et al., 2001), as observed in vivo (Paré, Shink, Gaudreau, Destexhe, & Lang, 1998). Otherwise, the network may fall in a synchronized regime, for example, in response to a step current, causing the population activity to oscillate around that predicted by the rate model.

Additional work is required to investigate the predictions of the time-varying model in more complex situations, as, for example, in populations of interacting neurons or in the case of voltage-gated, saturating conductances (as, e.g., NMDA-mediated). In the absence of adaptation, the predictions of the model have been shown to be good in these more complex cases as well (e.g., Renart et al., 2003). We expect no difference in performance when adaptation is included as done in section 3.

Appendix A: Model Neurons

A.1 Leaky Integrate-and-Fire Neuron. The leaky IF neuron is a single-compartment model characterized by its membrane voltage V and with a fixed threshold θ for spike emission. Upon crossing of θ from below, a spike is said to occur, and the membrane is clamped to a reset potential V_r for a refractory time τ_r, after which normal dynamics resume. We assume that a large number of postsynaptic potentials of small amplitude are required to reach the threshold. In such a condition, prevalent in the cortex, the subthreshold membrane dynamics can be assimilated to a continuous random walk, the Ornstein-Uhlenbeck (OU) process (this is the diffusion approximation; see, e.g., Lánský & Sato, 1999). Taking into account the effect of I_{alpp}, the subthreshold dynamics of the membrane potential obeys the stochastic differential equation,

$$dV = -\frac{V - V_{rest}}{\tau}dt + \mu dt + \sigma \xi_t \sqrt{dt}, \tag{A.1}$$

where

$$\mu = \frac{m + I_{alpp}}{C}, \qquad \sigma = \frac{\sqrt{2\tau' s}}{C}$$

are the average and standard deviation in unit time of the membrane voltage. m and s^2 are the average and the variance of the synaptic input current,

$I_{alp} = -g_N[N]_i$ (see equation 2.1), and $\sqrt{2\tau'}$ is a factor to preserve units (see, e.g., Rauch et al., 2003). $V_{rest} = 0$ is the resting potential, C is the capacitance of the membrane, $\tau = RC$, and R is the membrane resistance. ξ_t is a gaussian process with flat spectrum and unitary variance, $\langle \xi_t \xi_{t'} \rangle = \delta(t - t')$ (white noise; see, e.g., Tuckwell, 1988, or Gardiner, 1985, for more details). In a nonadapting neuron, $I_{alp} \equiv 0$. In the adapting threshold model (see section 2.2), $I_{alp} = 0$ and the threshold $\theta \geq \theta_0$ is a dynamical variable obeying equation 2.7.

A.2 Quadratic Integrate-and-Fire Neuron. The dimensionless variable V, to be interpreted as the membrane potential of the white noise–driven QIF neuron obeys

$$\tau dV = (V^2 + \mu)dt + \sigma \xi_t \sqrt{\tau dt}, \tag{A.2}$$

where τ is a time constant that mimics the effect of the membrane time constant, and μ, σ^2 are the average and variance per unit time of the input current. A spike is said to occur whenever $V = +\infty$, after which V is clamped to $V = -\infty$ for a refractory period τ_r. In practice, in the simulations, V is reset to -50 whenever $V = +50$. This gives an accurate approximation for the parameters chosen in Figure 2. On the other hand, in the rate function, equation 2.4, the actual values used for the integration limits do not matter, provided they are larger than $+10$ and smaller than -10 respectively.

A.3 Conductance-Based LIF Neuron. The membrane potential of the conductance-based LIF neuron obeys

$$dV = -\tilde{g}_L(V - V_{rest})dt + g_E(V_E - V)dP_E + g_I(V_I - V)dP_I,$$

where $g_{E,I} = \tau \bar{g}_{E,I}/C$ are dimensionless peak conductances, $\tilde{g}_L = 1/\tau$ is the leak conductance in appropriate units (1/ms), $V_{E,I}$ are the excitatory and inhibitory reversal potentials, and $dP_{E,I} = \sum_j \delta(t - t_j^{E,I})dt$ are Poisson spike trains with intensity $\nu_{E,I}$. In the diffusion approximation ($dP_x \to \nu_x dt + \sqrt{\nu_x dt}\xi_t$), the equation can be put in a form very similar to equation A.1 (see, e.g., Hanson & Tuckwell, 1983; Lánský & Lánská, 1987; Burkitt, 2001):

$$dV = -\frac{V}{\tau^*}dt + \mu_0 dt + \sigma_0(V)\sqrt{dt}\xi_t \tag{A.3}$$

where

$$\mu_0 = \tilde{g}_L V_{rest} + (g_E V_E \nu_E + g_I V_I \nu_I) \tag{A.4}$$

$$\sigma_0^2(V) = g_E^2(V_E - V)^2 \nu_E + g_I^2(V_I - V)^2 \nu_I \tag{A.5}$$

$$\tau^* = (\tilde{g}_L + g_E \nu_E + g_I \nu_I)^{-1}. \tag{A.6}$$

The main differences with respect to the current-based IF neuron are (1) the fluctuations depend on the membrane voltage; (2) an input-dependent, effective time constant τ^* appears; (3) the parameter μ_0 is *not* the average of the total input current (e.g., part of the input contributes to the leak term $-V/\tau^*$ and is not considered in μ_0); and (4) the voltage is bounded from below by the inhibitory reversal potential (below V_I, inhibitory inputs become excitatory). Usually the last point is taken care of by imposing a reflecting barrier R at V_I (Hanson & Tuckwell, 1983; Lánský & Lánská, 1987). The rate function of the CB neuron,

$$\Phi_{CB} = \left[\tau_r + \tau^* \int_{\frac{V_r-\mu_{ss}}{\sqrt{2}\sigma_{ss}}}^{\frac{\theta-\mu_{ss}}{\sqrt{2}\sigma_{ss}}} \sqrt{\pi} e^{x^2} (1 + \mathrm{erf}(x)) dx \right]^{-1}, \tag{A.7}$$

has been given in Burkitt et al. (2003) in the absence of a reflecting barrier. Figure 3 shows that in the typical case, it works also in the presence of a reflecting barrier at V_I. The constants μ_{ss}, σ_{ss}^2 appearing in equation A.7 are the stationary average and variance of the free (i.e., spikeless) membrane voltage, which are (Hanson & Tuckwell, 1983; Burkitt, 2001):

$$\mu_{ss} = \mu_0 \tau^* = \frac{\tilde{g}_L V_{rest} + (g_E V_E \nu_E + g_I V_I \nu_I)}{(\tilde{g}_L + g_E \nu_E + g_I \nu_I)} \tag{A.8}$$

and

$$\sigma_{ss}^2 = \frac{\tau^*}{2} \frac{\sigma_0^2(\mu_{ss})}{1-\eta} \approx \frac{\tau^*}{2} \sigma_0^2(\mu_{ss}), \tag{A.9}$$

where

$$\eta \equiv (g_E^2 \nu_E + g_I^2 \nu_I) \tau^*/2.$$

The approximation in equation A.9 follows from the fact that η is negligible in the typical case. For example, when $\bar{g}_{E,I} \sim 1$ nS, $C \sim 500$ pF, and $\nu_{E,I} \sim 10^3$ Hz, then $\eta \sim 10^{-4} - 10^{-3}$. (A convenient way to obtain the result, equation A.9, is to make use of the equality $\sigma_{ss}^2 = \tau^* \langle \sigma_0^2(V) \rangle / 2$, where the average $\langle . \rangle$ is taken on the free process. This is a generalization of a well-known property of the OU process in which σ_0 is constant.) equation A.7 can therefore be written as equation 2.6,

$$\Phi_{CB} = \left[\tau_r + \tau^* \int_{\frac{CV_r - m_0\tau^*}{s_0\sqrt{\tau^*}}}^{\frac{C\theta - m_0\tau^*}{s_0\sqrt{\tau^*}}} \sqrt{\pi} e^{x^2} (1 + \mathrm{erf}(x)) dx \right]^{-1},$$

where $m_0 \equiv C\mu_0$ and $s_0 \equiv C\sigma_0(\mu_{ss})$, so that m_0 has units of current:

$$m_0 = C\tilde{g}_L V_{rest} + C(g_E V_E \nu_E + g_I V_I \nu_I) \tag{A.10}$$

$$s_0^2 = C^2 g_E^2 (V_E - \mu_{ss})^2 \nu_E + C^2 g_I^2 (V_I - \mu_{ss})^2 \nu_I, \tag{A.11}$$

with μ_{ss} given by equation A.8 and $g_{E,I} \equiv \tau \bar{g}_{E,I}/C$. The adapted frequency is given by the solution of either $f = \Phi_{CB}(m_0 - \alpha f, s_0)$ (AHP-based model) or $f = \Phi_{CB}(\theta_0 + \beta f; m_0, s_0)$ (adapting threshold model).

Appendix B: Fitting Procedure

Here we briefly summarize the experimental procedure and the data analysis that led to the results of Table 1. Full details can be found in Rauch et al. (2003). Pyramidal neurons from layer 5 of rat somatosensory cortex were injected with an OU process with a correlation time constant $\tau' = 1$ ms to resemble white noise. Stimuli were delivered in random order from a preselected pool, which depended on the cell. The time length of the stimulus was between 6 and 12 seconds. The spike trains of 26 selected cells were analyzed to assess their mean spike frequencies. A transient ranging from 0.5 to 2 seconds (depending on stimulus duration) was discarded to deal with the stationary spike train only. On balance, the stationary response was usually adapted with respect to the transient one. The model rate functions were fitted to the experimental ones using a random least-square procedure, that is, a Monte Carlo minimization of the function (see, e.g., Press, Teukolsky, Vetterling, & Flannery, 1992),

$$\chi^2_{N-M} = \sum_{i=1}^{N} \left[\frac{\Phi_{MODEL}(m_i, s_i; \Pi) - f_i}{\Delta_i} \right]^2,$$

where i runs over the experimental points, f_i are the experimental spike frequencies, Π is the parameter set, and the weights Δ_i correspond approximately to a confidence interval of 68% for the output rate. M is the number of parameters to be tuned and N the number of experimental points. The best-fit was accepted if the probability of a variable χ^2_{N-M} to be larger than the observed $\chi^2_{\min}$ was larger than 0.01. The parameter set includes five parameters: τ_r, V_r, C, τ, and α [pA·s] for the AHP adaptation or β [mV·s] for the adapting threshold mechanism. Note that since Φ_{LIF}, equation 2.3, is invariant under the scaling $\theta \to \theta h$, $V_r \to V_r h$, $C \to C/h$ (h constant), only two out of these three parameters are independent. Therefore, the threshold for spike emission (θ_0 in the case of an adapting threshold) was set to 20 mV throughout. The results are summarized in Table 1 and discussed in the text.

Appendix C: The Effects of Adaptation on the LIF Neuron

Here we summarize and compare the properties of the LIF neuron endowed with the two models of adaptation, which are mentioned in the analysis of the experimental data in section 2.3. We will refer to the self-consistent solutions of equation 2.2 and 2.8 as $f_\alpha(m, s)$, $f_\beta(m, s)$, respectively. We consider the regions of low and intermediate-to-large rates in turn.

1. At low frequencies, the two models can be made equivalent by choosing $\beta C/\tau = \alpha$. This is because the response at rheobase, otherwise highly nonlinear, is linearized by either model of adaptation. One obtains

   $$f_{\alpha,\beta} \approx \rho_{\alpha,\beta}[m - m_{th}]_+$$

   as $m \to m_{th} = C\theta/\tau^+$, where m_{th} is the rheobase current, $\rho_\alpha = \alpha^{-1}$ for AHP adaptation, and $\rho_\beta = \tau/C\beta$ for adapting threshold. ($[x]_+ = x$ if $x > 0$ and zero otherwise, and $m \to y^+$ means that the limit is performed for values of m larger than y.) The linearization argument is due to Ermentrout (1998) for AHP-like adaptation and can be easily generalized to the case of an adapting threshold for the LIF neuron. The slope, ρ, can be obtained by looking at how the two forms of adaptation affect the rheobase $m_{th} = C\theta/\tau$, that is, by requiring that $m - \alpha f_\alpha - C\theta/\tau = m - C(\theta + \beta f_\beta)/\tau$. One finds $f_\alpha/f_\beta = C\beta/\alpha\tau$ so that for $C\beta = \alpha\tau$ the output frequencies at the rheobase (hence, the slopes of the linearized rate functions) are the same.

2. For $\tau_r = 0$, the rate functions of the two adapting models differ away from the rheobase. This can be seen most easily for large inputs, where the nonadapted response is approximately linear, $f \sim m/C(\theta - V_r)$. It is easy to derive that AHP adaptation preserves this linearity,

   $$f_\alpha \sim \frac{m}{C(\theta - V_r) + \alpha},$$

   while for an adapting threshold,

   $$f_\beta = \frac{(\theta - V_r)}{2\beta}\left(\sqrt{1 + \frac{4\beta m}{C(\theta - V_r)^2}} - 1\right), \tag{C.1}$$

   with asymptotic behavior $f_\beta \sim \sqrt{m/C\beta}$. The introduction of a finite refractory period makes the AHP model bend in this region,

   $$f_\alpha \sim \frac{1}{\tau_r}\left(1 - \frac{\alpha}{\tau_r m}\right),$$

   allowing the two models to match on the entire range of observed output rates.

Acknowledgments

We thank Paolo Del Giudice and Maurizio Mattia for useful discussions. This work was supported by the Swiss National Science Foundation (grants 31-61335.00 and 3152-065234.01) and the Silva Casa Foundation.

References

Abbott, L. F., & van Vreeswijk, C. (1993). Asynchronous states in networks of pulse-coupled oscillators. *Phys. Rev. E*, *48*, 1483–1490.

Amit, D. J., & Brunel, N. (1997). Model of global spontaneous activity and local structured (learned) delay activity during delay. *Cerebral Cortex, 7*, 237–252.

Amit, D. J., & Tsodyks, M. V. (1991). Quantitative study of attractor neural network retrieving at low spike rates: I. Substrate-spikes, rates and neuronal gain. *Network, 2*, 259–273.

Amit, D. J., & Tsodyks, M. V. (1992). Effective neurons and attractor neural networks in cortical environment. *Network, 3*, 121–137.

Brunel, N. (2000). Persistent activity and the single cell *f-I* curve in a cortical network model. *Network, 11*, 261–280.

Brunel, N., & Hakim, V. (1999). Fast global oscillations in networks of integrate-and-fire neurons with low firing rates. *Neural Computation, 11*, 1621–1671.

Brunel, N., & Latham, P. (2003). Firing rate of the noisy quadratic integrate-and-fire neuron. *Neural Computation, 15*, 2281–2306.

Brunel, N., & Sergi, S. (1998). Firing frequency of leaky integrate-and-fire neurons with synaptic currents dynamic. *J. Theor. Biol., 195*, 87–95.

Brunel, N., & Wang, X. J. (2001). Effects of neuromodulation in a cortical network model of object working memory dominated by recurrent inhibition. *Journal of Computational Neuroscience, 11*, 63–85.

Burkitt, A. N. (2001). Balanced neurons: Analysis of leaky integrate-and-fire neurons with reversal potentials. *Biol. Cybern., 85*, 247–255.

Burkitt, A. N., Meffin, H., & Grayden, D. B. (2003). Study of neuronal gain in a conductance-based leaky integrate-and-fire neuron model with balanced excitatory and inhibitory input. *Biol. Cybern., 89*, 119–125.

Chance, F. S., Abbott, L. F., & Reyes, A. D. (2002). Gain modulation from background synaptic input. *Neuron, 35*, 773–782.

Destexhe, A., Rudolph, M., Fellous, J. M., & Sejnowski, T. J. (2001). Fluctuating dynamic conductances recreate in-vivo like activity in neocortical neurons. *Neuroscience, 107*, 13–24.

Ermentrout, B. (1996). Type I membranes, phase resetting curves, and synchrony. *Neural Computation, 8*, 979–1001.

Ermentrout, B. (1998). Linearization of f-I curves by adaptation. *Neural Computation, 10*(7), 1721–1729.

Ermentrout, G. B., & Kopell, N. (1986). Parabolic bursting in an excitable system coupled with a slow oscillation. *SIAM J. Appl. Math., 46*, 233–253.

Fleidervish, I., Friedman, A., & Gutnick, M. J. (1996). Slow inactiavation of Na^+ current and slow cumulative spike adaptation in mouse and guinea-pig neocortical neurones in slices. *J. Physiol. (Cambridge), 493*, 83–97.

Fourcaud, N., & Brunel, N. (2002). Dynamics of the firing probability of noisy integrate-and-fire neurons. *Neural Computation, 14*, 2057–2110.

Fuhrmann, G., Markram, H., & Tsodyks, M. (2002). Spike frequency adaptation and neocortical rhythms. *J. Neurophysiology, 88*, 761–770.

Fusi, S., & Mattia, M. (1999). Collective behavior of networks with linear (VLSI) integrate and fire neurons. *Neural Computation, 11*, 633–652.

Gardiner, C. W. (1985). *Handbook of stochastic methods.* New York: Springer-Verlag.

Gerstner, W. (2000). Population dynamics of spiking neurons: Fast transients, asynchronous states, and locking. *Neural Computation, 12*, 43–90.

Hanson, F. B., & Tuckwell, H. C. (1983). Diffusion approximation for neural activity including synaptic reversal potentials. *J. Theor. Neurobiol., 2*, 127–153.

Holden, A. V. (1976). *Models of stochastic activity of neurons.* New York: Springer-Verlag.

Holt, G. R., & Koch, C. (1997). Shunting inhibition does not have a divisive effect on firing rates. *Neural Computation, 9*, 1001–1013.

Knight, B. W. (1972a). Dynamics of encoding of a population of neurons. *Journal of General Physiology, 59*, 734–736.

Knight, B. W. (1972b). The relationship between the firing rate of a single neuron and the level of activity in a network of neurons. Experimental evidence for resonance enhancement in the population response. *Journal of General Physiology, 59*, 767.

Lánský, P., & Lánská, V. (1987). Diffusion approximation of the neuronal model with synaptic reversal potentials. *Biol. Cybern., 56*, 19–26.

Lánský, P., & Sato, S. (1999). The stochastic diffusion models of nerve membrane depolarization and interspike interval generation. *Journal of the Peripheral Nervous System, 4*, 27–42.

Larkum, M., Senn, W., & Lüscher, H.-R. (in press). Top-down dendritic input increases the gain of layer 5 pyramidal neurons. *Cerebral Cortex*.

Liu, Y. H., & Wang, X. J. (2001). Spike-frequency adaptation of a generalized leaky integrate-and-fire model neuron. *Journal of Computational Neuroscience, 10*, 25–45.

Mattia, M., & Del Giudice, P. (2002). Population dynamics of interacting spiking neurons. *Phys. Rev. E, 66*, 051917.

McCormick, D. A., Connors, B. W., Lighthall, J. W., & Prince, D. (1985). Comparative electrophysiology of pyramidal and sparsely stellate neurons of the neocortex. *J. Neurophysiology, 54*, 782–806.

Moreno-Bote, R., & Parga, N. (2004a). *Membrane potential and response properties of populations of cortical neurons in the high conductance state*. Manuscript submitted for publication.

Moreno-Bote, R., & Parga, N. (2004b). Role of synaptic filtering on the firing response of simple model neurons. *Physical Review Letters, 92*, 028102.

Nykamp, D. Q., & Tranchina, D. (2000). A population density approach that facilitates large-scale modeling of neural networks: Analysis and an application to orientation tuning. *J. Comp. Neurosci., 8*, 19–30.

Paré, D., Shink, E., Gaudreau, H., Destexhe, A., & Lang, E. J. (1998). Impact of spontaneous synaptic activity on the resting properties of cat neocortical pyramidal neurons in vivo. *Journal of Neurophysiology, 11*, 1450–1460.

Poliakov, A. V., Powers, R. K., Sawczuk, A., & Binder, M. D. (1996). Effects of background noise on the response of rat and cat motoneurons to excitatory current transients. *Journal of Physiology, 495.1*, 143–157.

Powers, R. K., Sawczuk, A., Musick, J. R., & Binder, M. D. (1999). Multiple mechanisms of spike-frequency adaptation in motoneurones. *J. Physiol. (Paris), 93*, 101–114.

Press, W., Teukolsky, S. A., Vetterling, W. T., & Flannery, B. P. (1992). *Numerical recipes in C: The art of scientific computing*. Cambridge: Cambridge University Press.

Rauch, A., La Camera, G., Lüscher, H.-R., Senn, W., & Fusi, S. (2003). Neocortical cells respond as integrate-and-fire neurons to in vivo–like input currents. *J. Neurophysiol., 90*, 1598–1612.

Renart, A., Brunel, N., & Wang, X. J. (2003). Mean-field theory of recurrent cortical networks: From irregularly spiking neurons to working memory. In J. Feng (Ed.), *Computational neuroscience: A comprehensive approach*. Boca Raton, FL: CRC Press.

Ricciardi, L. M. (1977). *Diffusion processes and related topics in biology*. Berlin: Springer-Verlag.

Sah, P. (1996). Ca^{2+}-activated K^{+} currents in neurons: Types, physiological roles and modulation. *Trends Neurosci., 19*, 150–154.

Sanchez-Vives, M. V., Nowak, L. G., & McCormick, D. A. (2000). Cellular mechanisms of long-lasting adaptation in visual cortical neurons in vitro. *J. Neuroscience, 20*, 4286–4299.

Sawczuk, A., Powers, R. K., & Binder, M. D. (1997). Contribution of outward currents to spike frequency adaptation in hypoglossal motoneurons of the rat. *Journal of Physiology, 78*, 2246–2253.

Schwindt, P. C., & Crill, W. E. (1982). Factors influencing motoneuron rhythmic firing: Results from a voltage-clamp study. *J. Neurophysiol., 48*, 875–890.

Schwindt, P., O'Brien, J. A., & Crill, W. E. (1997). Quantitative analysis of firing properties of pyramidal neurons from layer 5 of rat sensorimotor cortex. *J. Neurophysiol., 77*, 2484–2498.

Schwindt, P. C., Spain, W. J., & Crill, W. E. (1989). Long-lasting reduction of excitability by a sodium-dependent potassium current in cat neocortical neurons. *J. Neurophysiol., 61*, 233–244.

Shadlen, M. N., & Newsome, W. T. (1998). The variable discharge of cortical neurons: Implications for connectivity, computation and information coding. *J. Neurosci., 18*, 3870–3896.

Shriki, O., Hansel, D., & Sompolinsky, H. (2003). Rate models for conductance-based cortical neural networks. *Neural Computation, 15*, 1809–1841.

Siegert, A. J. F. (1951). On the first passage time probability function. *Phys. Rev., 81*, 617–623.

Stafstrom, C. E., Schwindt, P. C., & Crill, W. E. (1984). Repetitive firing in layer V from cat neocortex in vitro. *J. Neurophysiol., 52*, 264–277.

Traub, R. D., & Miles, R. (1991). *Neuronal networks of the hippocampus*. Cambridge: Cambridge University Press.

Treves, A. (1993). Mean field analysis of neuronal spike dynamics. *Network, 4*, 259–284.

Tuckwell, H. C. (1988). *Introduction to theoretical neurobiology.* Cambridge: Cambridge University Press.

Wang, X. J. (1998). Calcium coding and adaptive temporal computation in cortical pyramidal neurons. *J. Neurophysiol., 79*, 1549–1566.

Wilbur, W. J., & Rinzel, J. (1983). A theoretical basis for large coefficient of variation and bimodality in neuronal interspike interval distribution. *J. Theor. Biol., 105*, 345–368.

Received March 28, 2003; accepted April 6, 2004.